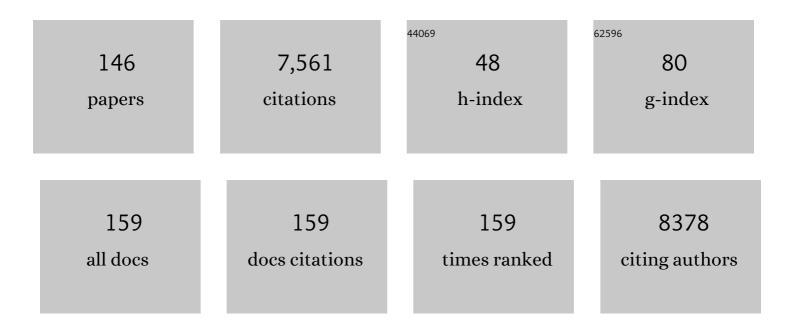
O V Safonova

List of Publications by Year in descending order

Source: https://exaly.com/author-pdf/5636623/publications.pdf Version: 2024-02-01



#	Article	IF	CITATIONS
1	Protagonists and spectators during photocatalytic solar water splitting with SrTaO _{<i>x</i>} N _{<i>y</i>} oxynitride. Journal of Materials Chemistry A, 2022, 10, 2374-2387.	10.3	10
2	Ru(III) single site solid micellar catalyst for selective aqueous phase hydrogenation of carbonyl groups in biomass-derived compounds. Applied Catalysis B: Environmental, 2022, 300, 120730.	20.2	12
3	Flame Spray Pyrolysis as a Synthesis Platform to Assess Metal Promotion in In ₂ O ₃ â€Catalyzed CO ₂ Hydrogenation. Advanced Energy Materials, 2022, 12, .	19.5	34
4	Redox Dynamics of Active VO <i>_x</i> Sites Promoted by TiO <i>_x</i> during Oxidative Dehydrogenation of Ethanol Detected by <i>Operando</i> Quick XAS. Jacs Au, 2022, 2, 762-776.	7.9	14
5	In situ study of low-temperature dry reforming of methane over La2Ce2O7 and LaNiO3 mixed oxides. Applied Catalysis B: Environmental, 2022, 315, 121528.	20.2	15
6	Elucidation of Metal Local Environments in Singleâ€Atom Catalysts Based on Carbon Nitrides. Small, 2022, 18, .	10.0	15
7	Assessing the environmental benefit of palladium-based single-atom heterogeneous catalysts for Sonogashira coupling. Green Chemistry, 2022, 24, 6879-6888.	9.0	10
8	CO2 hydrogenation on Cu-catalysts generated from ZnII single-sites: Enhanced CH3OH selectivity compared to Cu/ZnO/Al2O3. Journal of Catalysis, 2021, 394, 266-272.	6.2	35
9	Nanostructure of nickel-promoted indium oxide catalysts drives selectivity in CO2 hydrogenation. Nature Communications, 2021, 12, 1960.	12.8	90
10	Single-Atom-Substituted Mo ₂ C <i>T</i> _{<i>x</i>} :Fe-Layered Carbide for Selective Oxygen Reduction to Hydrogen Peroxide: Tracking the Evolution of the MXene Phase. Journal of the American Chemical Society, 2021, 143, 5771-5778.	13.7	61
11	Silica-Supported PdGa Nanoparticles: Metal Synergy for Highly Active and Selective CO ₂ -to-CH ₃ OH Hydrogenation. Jacs Au, 2021, 1, 450-458.	7.9	31
12	Potentialâ€Induced Spin Changes in Fe/N/C Electrocatalysts Assessed by In Situ Xâ€ray Emission Spectroscopy. Angewandte Chemie, 2021, 133, 11813-11818.	2.0	5
13	Lignin Compounds to Monoaromatics: Selective Cleavage of Câ^'O Bonds over a Brominated Ruthenium Catalyst. Angewandte Chemie - International Edition, 2021, 60, 12513-12523.	13.8	53
14	Potentialâ€Induced Spin Changes in Fe/N/C Electrocatalysts Assessed by In Situ Xâ€ray Emission Spectroscopy. Angewandte Chemie - International Edition, 2021, 60, 11707-11712.	13.8	36
15	Lignin Compounds to Monoaromatics: Selective Cleavage of Câ^O Bonds over a Brominated Ruthenium Catalyst. Angewandte Chemie, 2021, 133, 12621-12631.	2.0	10
16	Precursor Nuclearity and Ligand Effects in Atomicallyâ€Dispersed Heterogeneous Iron Catalysts for Alkyne Semiâ€Hydrogenation. ChemCatChem, 2021, 13, 3247-3256.	3.7	11
17	Deciphering the Phillips Catalyst by Orbital Analysis and Supervised Machine Learning from Cr Pre-edge XANES of Molecular Libraries. Journal of the American Chemical Society, 2021, 143, 7326-7341.	13.7	26
18	Following the structure of copper-zinc-alumina across the pressure gap in carbon dioxide hydrogenation. Nature Catalysis, 2021, 4, 488-497.	34.4	100

#	Article	IF	CITATIONS
19	Stable Palladium Oxide Clusters Encapsulated in Silicalite-1 for Complete Methane Oxidation. ACS Catalysis, 2021, 11, 7371-7382.	11.2	34
20	Enhanced Reducibility of the Ceria–Tin Oxide Solid Solution Modifies the CO Oxidation Mechanism at the Platinum–Oxide Interface. ACS Catalysis, 2021, 11, 9435-9449.	11.2	19
21	Surface molecular imprinting over supported metal catalysts for size-dependent selective hydrogenation reactions. Nature Catalysis, 2021, 4, 595-606.	34.4	52
22	Dynamics and Site Isolation: Keys to High Propane Dehydrogenation Performance of Silica-Supported PtGa Nanoparticles. Jacs Au, 2021, 1, 1445-1458.	7.9	32
23	Solid micellar Ru single-atom catalysts for the water-free hydrogenation of CO2 to formic acid. Applied Catalysis B: Environmental, 2021, 290, 120036.	20.2	43
24	Time-Resolved XAS Provides Direct Evidence for Oxygen Activation on Cationic Iron in a Bimetallic Pt-FeO <i>_x</i> /Al ₂ O ₃ Catalyst. ACS Catalysis, 2021, 11, 11793-11805.	11.2	16
25	Machine learning powered by principal component descriptors as the key for sorted structural fit of XANES. Physical Chemistry Chemical Physics, 2021, 23, 17873-17887.	2.8	7
26	Temperature and Reaction Environment Influence the Nature of Platinum Species Supported on Ceria. ACS Catalysis, 2021, 11, 13041-13049.	11.2	13
27	Silica-supported, narrowly distributed, subnanometric Pt–Zn particles from single sites with high propane dehydrogenation performance. Chemical Science, 2020, 11, 1549-1555.	7.4	77
28	Key activity descriptors of nickel-iron oxygen evolution electrocatalysts in the presence of alkali metal cations. Nature Communications, 2020, 11, 6181.	12.8	80
29	Carrierâ€Induced Modification of Palladium Nanoparticles on Porous Boron Nitride for Alkyne Semiâ€Hydrogenation. Angewandte Chemie, 2020, 132, 19807-19812.	2.0	11
30	Oxidative dehydrogenation of propane on silica-supported vanadyl sites promoted with sodium metavanadate. Catalysis Science and Technology, 2020, 10, 7186-7193.	4.1	2
31	Structure of copper sites in zeolites examined by Fourier and wavelet transform analysis of EXAFS. Chemical Science, 2020, 11, 5299-5312.	7.4	59
32	Low-Temperature Propylene Epoxidation Activity of CuO–CeO ₂ Catalyst with CO + O ₂ : Role of Metal–Support Interaction on the Reducibility and Catalytic Property of CuO _{<i>x</i>} Species. Journal of Physical Chemistry C, 2020, 124, 14131-14146.	3.1	20
33	Unwanted effects of X-rays in surface grafted copper(<scp>ii</scp>) organometallics and copper exchanged zeolites, how they manifest, and what can be done about them. Physical Chemistry Chemical Physics, 2020, 22, 6826-6837.	2.8	18
34	Elucidating the Oxygen Activation Mechanism on Ceria-Supported Copper-Oxo Species Using Time-Resolved X-ray Absorption Spectroscopy. ACS Catalysis, 2020, 10, 4692-4701.	11.2	21
35	Nanostructuring unlocks high performance of platinum single-atom catalysts for stable vinyl chloride production. Nature Catalysis, 2020, 3, 376-385.	34.4	122
36	Carrierâ€Induced Modification of Palladium Nanoparticles on Porous Boron Nitride for Alkyne Semiâ€Hydrogenation. Angewandte Chemie - International Edition, 2020, 59, 19639-19644.	13.8	36

#	Article	IF	CITATIONS
37	Enhanced CH ₃ OH selectivity in CO ₂ hydrogenation using Cu-based catalysts generated <i>via</i> SOMC from Ga ^{III} single-sites. Chemical Science, 2020, 11, 7593-7598.	7.4	30
38	Reducibility and Dispersion Influence the Activity in Silica-Supported Vanadium-Based Catalysts for the Oxidative Dehydrogenation of Propane: The Case of Sodium Decavanadate. ACS Catalysis, 2020, 10, 2314-2321.	11.2	22
39	CO 2 â€Promoted Catalytic Process Forming Higher Alcohols with Tunable Nature at Record Productivity. ChemCatChem, 2020, 12, 2732-2744.	3.7	14
40	Preserved in a Shell: Highâ€Performance Grapheneâ€Confined Ruthenium Nanoparticles in Acetylene Hydrochlorination. Angewandte Chemie, 2019, 131, 12425-12432.	2.0	5
41	Atomic-scale engineering of indium oxide promotion by palladium for methanol production via CO2 hydrogenation. Nature Communications, 2019, 10, 3377.	12.8	261
42	Ultra-Low-Temperature CO Oxidation Activity of Octahedral Site Cobalt Species in Co ₃ O ₄ Based Catalysts: Unravelling the Origin of the Unique Catalytic Property. Journal of Physical Chemistry C, 2019, 123, 19557-19571.	3.1	41
43	Preserved in a Shell: Highâ€Performance Grapheneâ€Confined Ruthenium Nanoparticles in Acetylene Hydrochlorination. Angewandte Chemie - International Edition, 2019, 58, 12297-12304.	13.8	53
44	Well-Defined Silica-Supported Tungsten(IV)–Oxo Complex: Olefin Metathesis Activity, Initiation, and Role of BrÃ,nsted Acid Sites. Journal of the American Chemical Society, 2019, 141, 18286-18292.	13.7	24
45	Zr(IV) surface sites determine CH3OH formation rate on Cu/ZrO2/SiO2 - CO2 hydrogenation catalysts. Chinese Journal of Catalysis, 2019, 40, 1741-1748.	14.0	22
46	Single Site Cobalt Substitution in 2D Molybdenum Carbide (MXene) Enhances Catalytic Activity in the Hydrogen Evolution Reaction. Journal of the American Chemical Society, 2019, 141, 17809-17816.	13.7	259
47	Controlling the speciation and reactivity of carbon-supported gold nanostructures for catalysed acetylene hydrochlorination. Chemical Science, 2019, 10, 359-369.	7.4	76
48	Atomâ€byâ€Atom Resolution of Structure–Function Relations over Lowâ€Nuclearity Metal Catalysts. Angewandte Chemie, 2019, 131, 8816-8821.	2.0	21
49	Atomâ€byâ€Atom Resolution of Structure–Function Relations over Lowâ€Nuclearity Metal Catalysts. Angewandte Chemie - International Edition, 2019, 58, 8724-8729.	13.8	108
50	Design of Single Gold Atoms on Nitrogenâ€Doped Carbon for Molecular Recognition in Alkyne Semiâ€Hydrogenation. Angewandte Chemie, 2019, 131, 514-519.	2.0	22
51	Design of Single Gold Atoms on Nitrogenâ€Doped Carbon for Molecular Recognition in Alkyne Semiâ€Hydrogenation. Angewandte Chemie - International Edition, 2019, 58, 504-509. Valence, exchange interaction, and location of Mn ions in polycrystalline <mml:math< td=""><td>13.8</td><td>111</td></mml:math<>	13.8	111
52	xmlns:mml="http://www.w3.org/1998/Math/MathML"> <mml:mrow><mml:mi mathvariant="normal">M<mml:msub><mml:mi mathvariant="normal">n<mml:mi>x</mml:mi><mml:msub><mml:mi mathvariant="normal">G<mml:msub><mml:mi< td=""><td>3.2</td><td>2</td></mml:mi<></mml:msub></mml:mi </mml:msub></mml:mi </mml:msub></mml:mi </mml:mrow>	3.2	2
53	mathvariant="normal">a <mml:mrow><mml:mn>1</mml:mn><mml:mo>â[*]</mml:mo>a[*]<mml:mi>xin situ XAFS study. Physical Chemistry Chemical Physics, 2018, 20, 5312-5318.</mml:mi></mml:mrow>	mml:mi>2.8	nml:mrow> <br 27
54	Effect of cobalt loading on structure and catalytic behavior of CoO x /SiO 2 in CO 2 -assisted	4.9	40

⁴ dehydrogenation of ethane. Applied Catalysis Á:	
--	--

4.3 48

#	Article	IF	CITATIONS
55	Identifying Dynamic Structural Changes of Active Sites in Pt–Ni Bimetallic Catalysts Using Multimodal Approaches. ACS Catalysis, 2018, 8, 4120-4131.	11.2	54
56	Silica-supported isolated molybdenum di-oxo species: formation and activation with organosilicon agent for olefin metathesis. Chemical Communications, 2018, 54, 3989-3992.	4.1	28
57	Application of valence-to-core X-ray emission spectroscopy for identification and estimation of amount of carbon covalently bonded to chromium in amorphous Cr-C coatings prepared by magnetron sputtering. Applied Surface Science, 2018, 427, 566-572.	6.1	6
58	Fluorescence-detected XAS with sub-second time resolution reveals new details about the redox activity of Pt/CeO ₂ catalyst. Journal of Synchrotron Radiation, 2018, 25, 989-997.	2.4	14
59	Kinetics of Lifetime Changes in Bimetallic Nanocatalysts Revealed by Quick Xâ€ray Absorption Spectroscopy. Angewandte Chemie - International Edition, 2018, 57, 12430-12434.	13.8	15
60	lsolated Zr Surface Sites on Silica Promote Hydrogenation of CO ₂ to CH ₃ OH in Supported Cu Catalysts. Journal of the American Chemical Society, 2018, 140, 10530-10535.	13.7	170
61	Highly Productive Propane Dehydrogenation Catalyst Using Silica-Supported Ga–Pt Nanoparticles Generated from Single-Sites. Journal of the American Chemical Society, 2018, 140, 11674-11679.	13.7	161
62	Kinetics of Lifetime Changes in Bimetallic Nanocatalysts Revealed by Quick Xâ€ r ay Absorption Spectroscopy. Angewandte Chemie, 2018, 130, 12610-12614.	2.0	2
63	C–H Activation and Proton Transfer Initiate Alkene Metathesis Activity of the Tungsten(IV)–Oxo Complex. Journal of the American Chemical Society, 2018, 140, 11395-11401.	13.7	21
64	Synthesis and Properties of Monolayer-Protected Co _{<i>x</i>} (SC ₂ H ₄ Ph) _{<i>m</i>} Nanoclusters. Journal of Physical Chemistry C, 2017, 121, 10948-10956.	3.1	14
65	Low-Temperature CO Oxidation over Combustion Made Fe- and Cr-Doped Co ₃ O ₄ Catalysts: Role of Dopant's Nature toward Achieving Superior Catalytic Activity and Stability. Journal of Physical Chemistry C, 2017, 121, 15256-15265.	3.1	67
66	Size-Selective Reactivity of Subnanometer Ag ₄ and Ag ₁₆ Clusters on a TiO ₂ Surface. Journal of Physical Chemistry C, 2017, 121, 6614-6625.	3.1	21
67	Silica-supported isolated gallium sites as highly active, selective and stable propane dehydrogenation catalysts. Chemical Science, 2017, 8, 2661-2666.	7.4	119
68	Introducing Time Resolution to Detect Ce ³⁺ Catalytically Active Sites at the Pt/CeO ₂ Interface through Ambient Pressure X-ray Photoelectron Spectroscopy. Journal of Physical Chemistry Letters, 2017, 8, 102-108.	4.6	80
69	Understanding the mechanism of synthesis of Pt ₃ Co intermetallic nanoparticles <i>via</i> preferential chemical vapor deposition. Journal of Materials Chemistry A, 2017, 5, 24396-24406.	10.3	21
70	Understanding the anomalous behavior of Vegard's law in Ce _{1â^'x} M _x O ₂ (M = Sn and Ti; 0 < x ≤0.5) solid solutions. Physical Chemistry Chemical Physics, 2016, 18, 13974-13983.	2.8	21
71	Low Temperature Activation of Supported Metathesis Catalysts by Organosilicon Reducing Agents. ACS Central Science, 2016, 2, 569-576.	11.3	65
72	Pushing up the magnetisation values for iron oxide nanoparticles via zinc doping: X-ray studies on the particle's sub-nano structure of different synthesis routes. Physical Chemistry Chemical Physics, 2016, 18, 25221-25229.	2.8	27

#	Article	IF	CITATIONS
73	X-ray emission spectroscopy: highly sensitive techniques for time-resolved probing of cerium reactivity under catalytic conditions. Physical Chemistry Chemical Physics, 2016, 18, 32486-32493.	2.8	11
74	C–H Activation on Co,O Sites: Isolated Surface Sites versus Molecular Analogs. Journal of the American Chemical Society, 2016, 138, 14987-14997.	13.7	117
75	Catalytically Active and Spectator Ce ³⁺ in Ceriaâ€&upported Metal Catalysts. Angewandte Chemie - International Edition, 2015, 54, 8728-8731.	13.8	168
76	Reply to Peters et al.: Proton transfers are plausible initiation and termination steps on Cr(III) sites in ethylene polymerization. Proceedings of the National Academy of Sciences of the United States of America, 2015, 112, E4162-3.	7.1	16
77	Chemical state of phosphorus in amorphous Ni–Fe–P electroplates. Surface and Coatings Technology, 2015, 275, 239-244.	4.8	17
78	Pd ₂ Au ₃₆ (SR) ₂₄ cluster: structure studies. Nanoscale, 2015, 7, 17012-17019.	5.6	46
79	Intracluster Atomic and Electronic Structural Heterogeneities in Supported Nanoscale Metal Catalysts. Journal of Physical Chemistry C, 2015, 119, 25615-25627.	3.1	9
80	Simultaneous generation of mild acidic functionalities and small supported Ir NPs from alumina-supported well-defined iridium siloxide. Journal of Catalysis, 2015, 321, 81-89.	6.2	24
81	Atomically dispersed rhodium on a support: the influence of a metal precursor and a support. Physical Chemistry Chemical Physics, 2014, 16, 26553-26560.	2.8	14
82	Bipyridine Periodic Mesoporous Organosilica: A Solid Ligand for the Iridium atalyzed Borylation of Cī£¿H Bonds. Advanced Synthesis and Catalysis, 2014, 356, 673-679.	4.3	47
83	Electronic and Geometric Structure of Ce ³⁺ Forming Under Reducing Conditions in Shaped Ceria Nanoparticles Promoted by Platinum. Journal of Physical Chemistry C, 2014, 118, 1974-1982.	3.1	34
84	Polymerization of Ethylene by Silica‣upported Dinuclear Cr ^{III} Sites through an Initiation Step Involving CH Bond Activation. Angewandte Chemie - International Edition, 2014, 53, 1872-1876.	13.8	120
85	Proton transfers are key elementary steps in ethylene polymerization on isolated chromium(III) silicates. Proceedings of the National Academy of Sciences of the United States of America, 2014, 111, 11624-11629.	7.1	118
86	Redox State Dynamics at the Surface of MoVTe(Sb)NbO M1 Phase in Selective Oxidation of Light Alkanes. Topics in Catalysis, 2013, 56, 1952-1962.	2.8	47
87	In situ hard X-ray quick RIXS to probe dynamic changes in the electronic structure of functional materials. Journal of Electron Spectroscopy and Related Phenomena, 2013, 188, 161-165.	1.7	29
88	Magnetic manipulation of molecules on a non-magnetic catalytic surface. Nanoscale, 2013, 5, 8462.	5.6	26
89	Fine tuning of gold electronic structure by IRMOF post-synthetic modification. RSC Advances, 2013, 3, 12043.	3.6	12
90	Oxidation State of Ce in CeO ₂ -Promoted Rh/Al ₂ O ₃ Catalysts during Methane Steam Reforming: H ₂ O Activation and Alumina Stabilization. ACS Catalysis, 2013, 3, 1956-1964.	11.2	44

#	Article	IF	CITATIONS
91	Effect of heat treatment on the electrocatalytic properties of nano-structured Ru cores with Pt shells. Journal of Electroanalytical Chemistry, 2013, 704, 57-66.	3.8	14
92	Infrared Studies on Bimetallic Copper/Nickel Catalysts Supported on Zirconia and Ceria/Zirconia. Catalysis Letters, 2013, 143, 517-530.	2.6	74
93	Subsecond and in Situ Chemical Speciation of Pt/Al ₂ O ₃ during Oxidation–Reduction Cycles Monitored by High-Energy Resolution Off-Resonant X-ray Spectroscopy. Journal of the American Chemical Society, 2013, 135, 19071-19074.	13.7	43
94	Application Ce L ₁ HERFD XAS to determine the atomic structure of CeO ₂ based nano-catalysts under working conditions. Journal of Physics: Conference Series, 2013, 430, 012062.	0.4	4
95	High energy resolution off-resonant spectroscopy at sub-second time resolution: (Pt(acac)2) decomposition. Chemical Communications, 2012, 48, 10898.	4.1	48
96	Scientific Opportunities for Heterogeneous Catalysis Research at the SuperXAS and SNBL Beam Lines. Chimia, 2012, 66, 699.	0.6	60
97	The oxidation state of copper in bimetallic (Pt–Cu, Pd–Cu) catalysts during water denitration. Catalysis Science and Technology, 2012, 2, 794.	4.1	32
98	Structure of the methanol synthesis catalyst determined by in situHERFD XAS and EXAFS. Catalysis Science and Technology, 2012, 2, 373-378.	4.1	33
99	Sulfidation Mechanism of Pure and Cu-Doped ZnO Nanoparticles at Moderate Temperature: TEM and In Situ XRD Studies. Journal of Physical Chemistry C, 2012, 116, 14423-14430.	3.1	30
100	On the State of Pd in Perovskite-Type Oxidation Catalysts of Composition A(B,Pd)O _{3±δ} (A =) Tj ETO	Qq0 0 0 r 6.7	gBT /Overloc
101	A von Hamos x-ray spectrometer based on a segmented-type diffraction crystal for single-shot x-ray emission spectroscopy and time-resolved resonant inelastic x-ray scattering studies. Review of Scientific Instruments, 2012, 83, 103105.	1.3	158
102	Polyhedral CeO ₂ Nanoparticles: Size-Dependent Geometrical and Electronic Structure. Journal of Physical Chemistry C, 2012, 116, 7312-7317.	3.1	108
103	Redispersion of Gold Multiple-Twinned Particles during Liquid-Phase Hydrogenation. ACS Catalysis, 2012, 2, 1394-1403.	11.2	29
104	Evolution of structural properties of iron oxide nano particles during temperature treatment from 250°C–900°C: X-ray diffraction and Fe K-shell pre-edge X-ray absorption study. Current Applied Physics, 2012, 12, 817-825.	2.4	80
105	Study of N-bridged diiron phthalocyanine relevant to methane oxidation: Insight into oxidation and spin states from high resolution 1s core hole X-ray spectroscopy. Applied Catalysis B: Environmental, 2012, 113-114, 43-51.	20.2	18
106	SNBL, a dedicated beamline for combined <i>in situ</i> X-ray diffraction, X-ray absorption and Raman scattering experiments. Phase Transitions, 2011, 84, 726-732.	1.3	107
107	Structure and catalytic performance of Pt-promoted alumina-supported cobalt catalysts under realistic conditions of Fischer–Tropsch synthesis. Journal of Catalysis, 2011, 277, 14-26.	6.2	211
108	Identification of the active species in the working alumina-supported cobalt catalyst under various	4.4	87

conditions of Fischer–Tropsch synthesis. Catalysis Today, 2011, 164, 62-67.

#	Article	IF	CITATIONS
109	2.8NiO–H1.8Ni0.6(OH)MoO4—Novel nanocomposite material for the reactive adsorption of sulfur-containing molecules at moderate temperature. Applied Catalysis B: Environmental, 2011, 106, 460-468.	20.2	6
110	Elucidation of the chemical state of phosphorus and boron in crystallographically amorphous nickel electroplates. Russian Journal of Electrochemistry, 2010, 46, 1223-1229.	0.9	8
111	In Situ XRD Detection of Reversible Dawsonite Formation on Alkali Promoted Alumina: A Cheap Sorbent for CO ₂ Capture. European Journal of Inorganic Chemistry, 2010, 2010, 2461-2464.	2.0	23
112	High CO ₂ Storage Capacity in Alkaliâ€Promoted Hydrotalciteâ€Based Material: In Situ Detection of Reversible Formation of Magnesium Carbonate. Chemistry - A European Journal, 2010, 16, 12694-12700.	3.3	51
113	Chemical composition and structural transformations of amorphous chromium coatings electrodeposited from Cr(III) electrolytes. Electrochimica Acta, 2010, 56, 145-153.	5.2	61
114	Stability and Reactivity of ϵⴒχⴴÎ, Iron Carbide Catalyst Phases in Fischerâ^'Tropsch Synthesis: Controlling μ _C . Journal of the American Chemical Society, 2010, 132, 14928-14941.	13.7	426
115	The Effect of the State of Pd on Methane Combustion in Pd-Doped LaFeO ₃ . Journal of Physical Chemistry C, 2010, 114, 4584-4594.	3.1	78
116	In situXRD investigation of the evolution of alumina-supported cobaltcatalysts under realistic conditions of Fischer-Tropsch synthesis. Chemical Communications, 2010, 46, 788-790.	4.1	110
117	Local environment of vanadium in V/Al/O-mixed oxide catalyst for propane ammoxidation: Characterization by in situ valence-to-core X-ray emission spectroscopy and X-ray absorption spectroscopy. Journal of Catalysis, 2009, 268, 156-164.	6.2	29
118	In situ XAS with high-energy resolution: The changing structure of platinum during the oxidation of carbon monoxide. Catalysis Today, 2009, 145, 300-306.	4.4	29
119	Reaction between Thiophene and Ni Nanoparticles Supported on SiO ₂ or ZnO: In Situ Synchrotron X-ray Diffraction Study. Journal of Physical Chemistry C, 2009, 113, 17064-17069.	3.1	36
120	Decomposition of Carbon Dioxide at 500 °C over Reduced Iron, Cobalt, Nickel, and Zinc Ferrites: A Combined XANESâ^'XRD Study. Journal of Physical Chemistry C, 2009, 113, 19568-19577.	3.1	25
121	Cr local environment by valence-to-core X-ray emission spectroscopy. Journal of Analytical Atomic Spectrometry, 2009, 24, 215-223.	3.0	52
122	A high-temperature furnace for <i>in situ</i> synchrotron X-ray spectroscopy under controlled atmospheric conditions. Journal of Synchrotron Radiation, 2008, 15, 489-494.	2.4	10
123	Generating Highly Active Partially Oxidized Platinum during Oxidation of Carbon Monoxide over Pt/Al ₂ O ₃ : In Situ, Timeâ€Resolved, and Highâ€Energyâ€Resolution Xâ€Ray Absorption Spectroscopy. Angewandte Chemie - International Edition, 2008, 47, 9260-9264.	13.8	119
124	Hard X-Ray Photon-In-Photon-Out Spectroscopy with Lifetime Resolution — of XAS, XES, RIXSS and HERFD. AIP Conference Proceedings, 2007, , .	0.4	4
125	High Energy Resolution Fluorescence Detection X-Ray Absorption Spectroscopy: Detection of Adsorption Sites in Supported Metal Catalysts. AIP Conference Proceedings, 2007, , .	0.4	8
126	High-Throughput Structure/Function Screening of Materials and Catalysts with Multiple Spectroscopic Techniques. AIP Conference Proceedings, 2007, , .	0.4	3

#	Article	IF	CITATIONS
127	Application of In-Situ High Energy-Resolution Fluorescence Detection and Time-Resolved X-Ray Spectroscopy: Catalytic Activation of Oxygen over Supported Gold Catalysts. AIP Conference Proceedings, 2007, , .	0.4	0
128	Buildup of the InSe/M interface (MPd, Au) studied by X-ray photoemission and X-ray absorption spectroscopy. Surface Science, 2007, 601, 3778-3783.	1.9	6
129	The nature of the active site in the Fe-ZSM-5/N2O system studied by (resonant) inelastic X-ray scattering. Catalysis Today, 2007, 126, 127-134.	4.4	49
130	Mechanism of the Oxidationâ~'Reduction of the MoVSbNbO Catalyst:Â In Operando X-ray Absorption Spectroscopy and Electrical Conductivity Measurements. Journal of Physical Chemistry B, 2006, 110, 23962-23967.	2.6	55
131	Site preference and local geometry of Sc in garnets: Part II. The crystal-chemistry of octahedral Sc in the andradite-Ca3Sc2Si3O12 join. American Mineralogist, 2006, 91, 1240-1248.	1.9	32
132	On the Presence of Fe(IV) in Fe-ZSM-5 and FeSrO3-xUnequivocal Detection of the 3d4Spin System by Resonant Inelastic X-ray Scattering. Journal of Physical Chemistry B, 2006, 110, 18104-18107.	2.6	36
133	Valence-to-Core X-ray Emission Spectroscopy Identification of Carbide Compounds in Nanocrystalline Cr Coatings Deposited from Cr(III) Electrolytes Containing Organic Substances. Journal of Physical Chemistry B, 2006, 110, 23192-23196.	2.6	104
134	Identification of CO Adsorption Sites in Supported Pt Catalysts Using High-Energy-Resolution Fluorescence Detection X-ray Spectroscopy. Journal of Physical Chemistry B, 2006, 110, 16162-16164.	2.6	163
135	Activation of Oxygen on Gold/Alumina Catalysts: In Situ High-Energy-Resolution Fluorescence and Time-Resolved X-ray Spectroscopy. Angewandte Chemie - International Edition, 2006, 45, 4651-4654.	13.8	208
136	Buildup and structure of theInSeâ^•Ptinterface studied by angle-resolved photoemission and x-ray absorption spectroscopy. Physical Review B, 2006, 73, .	3.2	7
137	Characterization of the H2 sensing mechanism of Pd-promoted SnO2 by XAS in operando conditions. Chemical Communications, 2005, , 5202.	4.1	30
138	Dopants in nanocrystalline tin dioxide. Russian Chemical Bulletin, 2003, 52, 1217-1238.	1.5	68
139	Mechanism of sensing CO in nitrogen by nanocrystalline SnO2 and SnO2(Pd) studied by Mössbauer spectroscopy and conductance measurements. Journal of Materials Chemistry, 2002, 12, 1174-1178.	6.7	49
140	CO and NO2 gas sensitivity of nanocrystalline tin dioxide thin films doped with Pd, Ru and Rh. Materials Science and Engineering C, 2002, 21, 105-111.	7.3	110
141	Sensor Properties of Pd-Doped SnO2 Films Deposited by Laser Ablation. Inorganic Materials, 2002, 38, 374-379.	0.8	11
142	Effect of combined Pd and Cu doping on microstructure, electrical and gas sensor properties of nanocrystalline tin dioxide. Materials Science and Engineering B: Solid-State Materials for Advanced Technology, 2001, 85, 43-49.	3.5	56
143	Two successive effects in the interaction of nanocrystalline SnO2 thin films with reducing gases. Materials Science and Engineering B: Solid-State Materials for Advanced Technology, 2000, 77, 159-166.	3.5	21
144	Laser ablation doping of poly crystalline tin dioxide films with palladium. High Energy Chemistry, 2000, 34, 182-187.	0.9	2

#	Article	IF	CITATIONS
145	Effect of doping metals on the kinetics of interaction of SnO2 thin films with oxygen. Journal of Materials Chemistry, 1998, 8, 1577-1581.	6.7	4
146	Thermodynamical analysis of non-stoichiometric thallium oxides and reactivity prediction for electrosynthesis. Electrochimica Acta, 1997, 42, 2943-2946.	5.2	5